Volume 1 | Number 1 | Jan 2013 | Pages 1–100

Journal of
Materials Chemistry A

Materials for energy and sustainability
www.rsc.org/materialsA

Li⁺

ROYAL SOCIETY
OF CHEMISTRY

ROYAL SOCIETY
OF CHEMISTRY

www.rsc.org/materialsA

ARTICLE

Electrospinning Hierarchical LiV$_3$O$_8$ Nanowire-in-Network for High-Rate and Long-Life Lithium Batteries†

Wenhao Ren,‡ Zhiping Zheng,‡ Yanzhu Luo, Wei Chen,* Chaojiang Niu, Kangning Zhao, Mengyu Yan, Lei Zhang, Jiashen Meng, and Liqiang Mai*

Structural and morphological control of LiV$_3$O$_8$ material has a significant impact on its electrochemical performance. In order to obtain a favorable structure, a hierarchical LiV$_3$O$_8$ nanowire-in-network is designed and constructed by electrospinning through polymer crosslinking strategy. The crosslinking effect between poly (vinyl alcohol) (PVA) and poly (ethylene oxide) (PEO) not only benefits for electrospinning, but also realizes a mild multi-step degradation process during calcination. Based on temperature-dependent experiments and thermogravimetric (TG) analysis, the function of polymer blends and the formation mechanism of the structure are discussed in detail. As a cathode for lithium battery, the LiV$_3$O$_8$ exhibits a high initial capacity of 320.6 mA h g^{-1} at 100 mA g^{-1} and a high-rate capacity of 202.8 mA h g^{-1} at 2000 mA g^{-1}. This remarkable performance is attributed to the unique structure, which provides large effective contact area, low charge transfer resistance, and improved structure stability. Our work indicates that the hierarchical LiV$_3$O$_8$ nanowire-in-network material is a promising cathode for use in high-rate and long-life rechargeable lithium batteries.

Introduction

Lithium batteries (LBs) have attracted extensive attention in portable electronic devices and electric vehicles owing to its high energy density and long cycle life. For further widespread application, significant efforts should be made to reduce the cost and improve the electrochemical performance.[1-10] The layered lithium trivanadate (LiV$_3$O$_8$) cathode material has attracted considerable attention due to its low cost, abundant source, high energy density, and good safety feature.[11-15] Despite a variety of methods have been developed for the synthesis of LiV$_3$O$_8$ in recent years, it still suffers from unsatisfactory capacity loss and poor rate capability because of the incomplete phase transformation, slow electrode kinetics, and structural degradation.[16-21]

State Key Laboratory of Advanced Technology for Materials Synthesis and Processing, Wuhan University of Technology, Hubei, Wuhan 430070, China. E-mail: mlq518@whut.edu.cn; chenwei_juan@sina.com
†Electronic Supplementary Information (ESI) available: FTIR spectra, TEM images, SAED patterns, FESEM images, TG image of the samples, charge-discharge curves and differential capacity *vs*. voltage curves of LVO-PVA/PEO at different cycles, related photographs of the synthesis processes of the samples. See DOI: 10.1039/x0xx00000x
‡ These authors contributed equally to this work.

It has been reported that the electrochemical performance of LiV$_3$O$_8$ is influenced by the morphology significantly.[22] The rational design of LiV$_3$O$_8$ with favorable structure is of great importance. Nanostructure materials with specific architecture such as hierarchical nanowire not only provide extra tunnels for fast ion diffusion, but also effectively prevent the self-aggregation of nanomaterials during charge/discharge processes. Furthermore, the formation of network structure can further improve the stability and electronic conduction of hierarchical nanowires.[23-25] Therefore, the network architecture consisted of hierarchical nanowires is a favorable structure for high performance lithium batteries.

It is worth noting that electrospinning has been widely recognized as a convenient and cost-effective method to generate a variety of nanowires with unique morphologies.[26-29] However, typical electrospinning technique could only obtain the nanowires with simple morphology and the design of unique structure is still a challenge. Herein, we propose a crosslinking strategy via controlled electrospinning to construct hierarchical LiV$_3$O$_8$ nanowire-in-network. This strategy takes advantage of the characteristics of different polymers, which influences spinning performance and pyrolysis features. Based on the method, a mild multi-step degradation process during calcination is achieved, thus in favor of the formation of the structure. The continuous morphological development of LiV$_3$O$_8$ (Fig. 1) mainly include three stages, from smooth nanofibers to hierarchical nanowires, and finally nanowire-in-network structure. This unique architecture can provide continuous
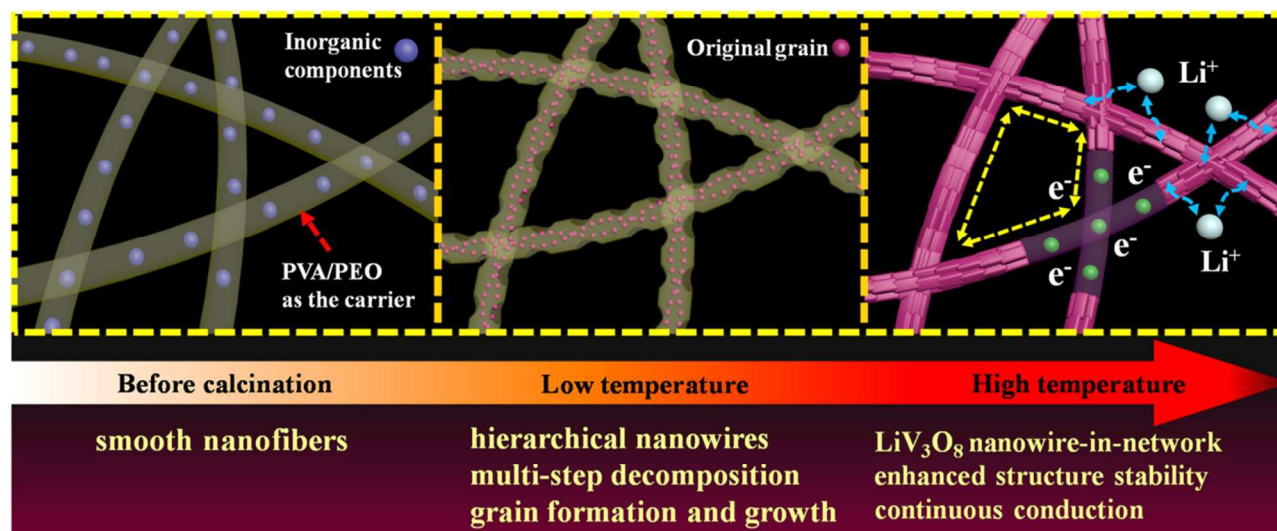
Fig. 1 Schematic illustration of the proposed formation mechanism of the hierarchical LiV_3O_8 naowire-in-network during calcination.

electronic conduction and extra tunnels for efficient contact between LiV_3O_8 and electrolyte, affording low charge transfer resistance and high specific capacity. It is expected that the crosslinking strategy in electrospinning could be extended to the preparation of other nanomaterials with unique architectures.

Experimental Section

Material synthesis

For a typical synthesis, ammonium metavanadate (NH_4VO_3, 0.528 g), lithium acetate (LiAc, 0.161 g), PEO (0.9 g, M_W = 400,000), and PVA (0.9 g, $M_W \approx 65,000$) were dissolved in 30 ml distilled water with stirring at 80 °C for 6 h. A light-yellow clear solution was obtained with a certain viscosity. Then, the precursor solution was loaded into a plastic syringe and injected at a constant flow rate of 0.5 mL h^{-1}. The spinning voltage was set at 20 kV and the distance between collector and spinneret was 15 cm. Finally, the as-prepared nanofibers with aluminum foil were annealed at 400 °C in air for 5 h to obtain a brown powder. For comparison, the samples were also synthesized by using PVA or PEO individually. The final products synthesized through PVA, PEO, or PVA/PEO was marked as LVO-PVA, LVO-PEO, and LVO-PVA/PEO, respectively.

Materials characterization

X-ray diffraction (XRD) measurement was performed to investigate the crystallographic information using a D8 Advance X-ray diffractometer with non-monochromated Cu Kα X-ray source. Fourier transformed infrared (FTIR) transmittance spectra were recorded using the 60-SXB IR spectrometer. Field emission scanning electron microscopic (FESEM) images were collected with a JEOL JSM-7100F at an acceleration voltage of 10 kV. Transmission electron microscopy (TEM) and high-resolution TEM (HRTEM) images were recorded with a JEM-2100F microscope. TG analysis was performed using NETZSCH-STA449c/3/G thermoanalyzer.

Electrochemical measurements

The electrochemical measurements were tested with 2025 coin cells assembled in a glove box filled with pure argon. Lithium foil was used as the anode and 1 M solution of $LiPF_6$ in ethylene carbon (EC)/dimethyl carbonate (DMC) was used as the electrolyte. Cathode electrodes were produced with 70 wt.% LiV_3O_8 active material, 20 wt.% acetylene black and 10 wt.% poly (tetrafluoroethylene) (PTFE). The battery was aged for 24 h before test to ensure full absorption of the electrolyte into the electrodes. The mass loading of the active material was 3-4 mg cm^{-2}. Galvanostatic charge/discharge measurement was performed in the potential range from 1.5 to 4 V $vs.$ Li/Li$^+$ with a multichannel battery testing system (LAND CT2001A). Cyclic voltammetry (CV) and electrochemical impedance spectroscopy (EIS) were performed with an electrochemical workstation (Autolab PGSTAT302N).

Results and discussion

The X-ray diffraction (XRD) measurements were conducted to determine the phase structures of the samples. As shown in Fig. 2a, all the prepared materials are indexed to the layered monoclinic LiV_3O_8 phase (JCPDS card no. 72-1193, space group: P21/m), which is consistent with previous reports.[11, 30] Moreover, the peak positions and the peak intensities of sample LVO-PVA, LVO-PEO, and LVO-PVA/PEO are similar, suggesting that the polymer component does not significantly change the crystal structure of LiV_3O_8. Then, FTIR spectroscopy of LVO-PVA/PEO was applied to further investigate the structural change in bonding (Fig. 2b). Before annealing, the strong bands observed between 500 and 2000 cm^{-1} can be assigned to bending and stretching vibrations of PVA and PEO. The band at 2888 cm^{-1} is attributed to the vibrations of -CH$_2$-.[14] Notably, the hydroxyl stretching band of LVO-PVA/PEO at 3416 cm^{-1} is higher than LVO-PVA at 3400 cm^{-1} but lower than LVO-PEO at 3431 cm^{-1} (Fig. S2†),
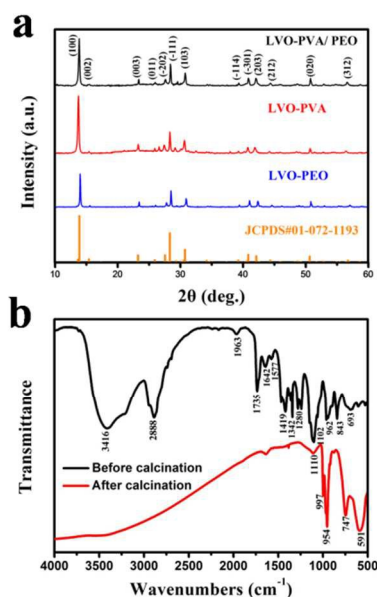
Fig. 2 (a) XRD patterns of LVO-PVA/PEO, LVO-PVA, and LVO-PEO. (b) FTIR spectra of electrospun LVO-PVA/PEO composite before and after calcination.

indicating that the intra- and inter- molecular interactions among PVA have been weakened by crosslinking with PEO and the newly formed hydrogen bonds are stronger.[31] After annealing, the bands belong to PVA and PEO disappeared; instead, well defined features of LiV_3O_8 are observed. The bands at 997 and 954 cm^{-1} are assigned to the vibrations of V=O. The band at 747 cm^{-1} is attributed to stretching vibrations of V-O-V and peaks between 600 and 400 cm^{-1} are attributed to the bending vibrations of V-O-V and V=O.[17, 32, 33]

SEM and TEM were used to characterize the morphology and detailed structure of the samples. Fig. 3 shows the SEM images of electrospun nanofibers of LVO-PVA/PEO, LVO-PVA, and LVO-PEO before and after calcination at 400 °C. All the electrospun nanofibers are smooth and uniform before annealing; the diameter distribution of LVO-PVA/PEO, LVO-PVA, and LVO-PEO are centered at 200, 450, and 110 nm, respectively. Notably, the diameter of electrospun nanowire decreases with the increment of the PEO content. This is because that the addition of PEO can weaken the hydrogen bonds in PVA molecules, thus inhibits the crystallization and increase the nucleation points of PVA, therefore promote the movability of PVA molecular chains under electrostatic force.[31]

Interestingly, only LVO-PVA/PEO can form hierarchical nanowire-in-network structure after the heat-treatment. The length of the nanowires is up to several millimeters; the width and length of each attached nanorods are around 50 and 150 nm, respectively. However, the morphologies of LVO-PVA and LVO-PEO are self-aggregated and mainly composed of detached nanorods with irregular structure. A irregular morphology similar to that of LVO-PVA has also been reported by Kwang-Pill Lee et al. via electrospinning.[34] TEM images show that the LVO-PVA/PEO nanowires and nanorods (Fig. 4a and 4b) are tightly connected with each other. The Fast Fourier Transformation (FFT) patterns (Fig. 4d) indicate that the edge of nanowire is single-crystalline and well-defined in crystal phase. Fig. 4e also reveals that there exist two sets of lattices in connected region and further confirms the particles have grown together and formed the grain. The lattice spacing of 11.52 Å shown in HRTEM image (Fig. S3†) corresponds to the (001) interplanar distance of LiV_3O_8 (JCPDS card no. 72-1193). The SAED pattern reveals the well-defined orientation of the nanorod and the axial direction is [$\bar{3}01$].

Most importantly, unlike typical preparation for sol precursor that only based on one sort of polymer (PVA, PVP or PEO etc.), we select two complementary polymers to achieve a better electrospinning process. On the one hand, the use of PVA can
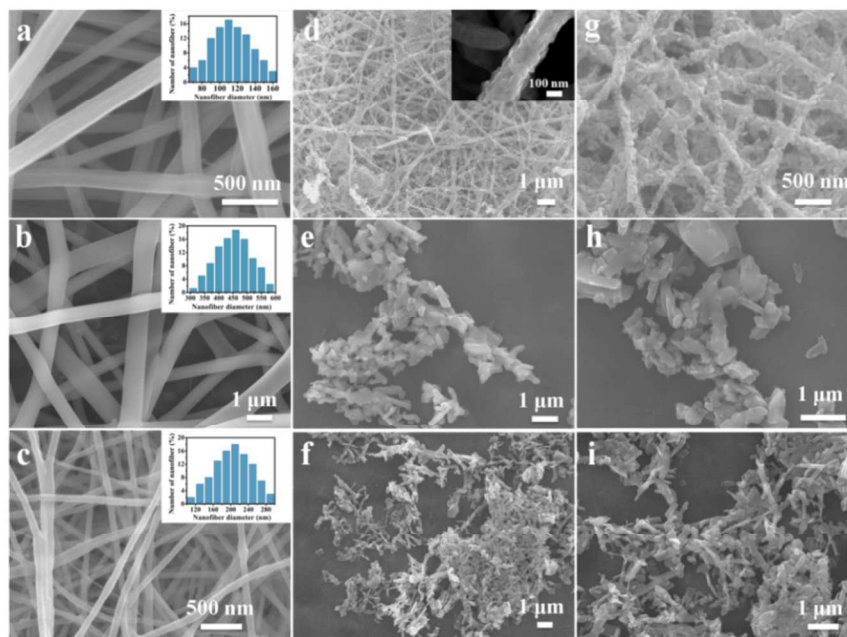
Fig. 3 SEM images of electrospun LVO-PVA/PEO (a), LVO-PVA (b) and LVO-PEO (c) before annealing. Insets of (a-c) are the corresponding diameter distribution diagram. SEM images of LVO-PVA/PEO (d and g), LVO-PVA (e and h) and LVO-PEO (f and i) after annealing. Inset of (d) is the SEM image of a single LVO-PVA/PEO nanowire.
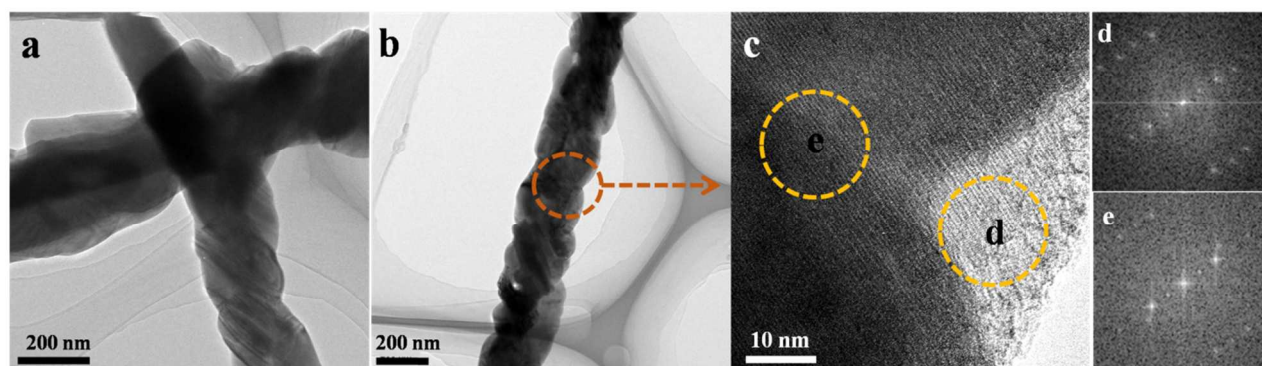
Fig. 4 TEM images (a and b), HRTEM image (c) and FFT patterns (d and e) of hierarchical LVO-PVA/PEO nanowire.

promote both the electrical conductivity of the solution and the mechanical properties of the spinning. However, the melting point of PVA is close to its decomposition temperature, resulting in poor processability and fierce decomposition process. Besides, PVA molecules possess high hydrophilicity, and high concentration of PVA solution seriously affects solvent volatilization and easy to separate out during electrospinning.[35, 36] On the other hand, the addition of PEO can weaken the intra- and inter-molecular hydrogen bonds of PVA, change the aggregation states of PVA chains, and decrease its melting point and crystallinity. Then the movability of PVA molecular chains is promoted and become liable to extend under the outside force. Thus the spin is easy to form and the diameter of electrospun nanofiber becomes smaller.[31, 37, 38] Moreover, PVA and PEO also served as a carrier and effectively prevent the self-aggregation of the nanorods during heat-treatment process.

Although some similar formation mechanisms were investigated by other researchers,[39] the function of polymer blends for constructing hierarchical structure was ignored. Therefore, the temperature-dependent experiments combined with TG analysis were conducted to gain further insight into the formation mechanism of the LiV_3O_8 network structure. The continuous morphological evolution of sample LVO-PVA/PEO (Fig. 1) mainly includes three stages, from smooth nanofibers to hierarchical nanowires, and finally nanowire-in-network structure. In the first stage, the smooth nanofibers start to degrade and become rough. A mass loss of about 7.56 wt.% is observed on the TG curve (Fig. 5a) from 100 °C to 170 °C due to the oxidation and dehydration of electrospun LVO-PVA/PEO composite. The first two peaks indicated in differential scanning calorimetry (DSC) at 67 °C and 150 °C are attributed to the T_m (melting temperature) and initial degradation of PVA. In the second stage, the nucleary of original LiV_3O_8 grain and the decomposition of polymer occur simultaneously so that hierarchical nanowires are formed (Fig. S4†). The composite was further oxidized with a 51.47 wt.% mass loss from 170 °C to 265 °C. This mass loss is mainly attributed to the decomposition of PVA as can be deduced from the DSC curve of LVO-PVA. (Fig. 5b, red curve). Notably, the DSC peak of LVO-PVA at 253 °C is much higher than LVO-PVA/PEO at 240 °C. Thus, the reaction intensity of LVO-PVA/PEO becomes mild due to the use of PEO. Besides, PEO is still stable at this stage and helps to maintain the basic structure of LVO-PVA/PEO, so the decomposition of PVA would not destroy the structure significantly. In the third stage, the small LiV_3O_8 particles gradually grow into connected nanorods and replace polymer components as the carrier for constructing

hierarchical nanowire-in-network structure. The 18.51 wt.% mass loss from 265 °C to 445 °C is due to the completely decomposition of polymer. Similarly, the reaction intensity of LVO-PVA/PEO is lower than LVO-PEO in this temperature interval. As the calcination temperature increased to 450 °C, the size of LiV_3O_8 nanorods grow much bigger and it consumes a large number of connected materials. Thus the self-aggregation of nanorods occurs and the hierarchical naowire-in-network structure cannot be maintained (Fig. S5†). In summary, only LVO-PVA/PEO can form the unique hierarchical structure under controlled calcination. This is attributed to the different pyrolysis properties of PVA and PEO, thus a mild multi-step degradation process is achieved via polymer crosslinking; in this way a gentle heat-treatment process is ensured.
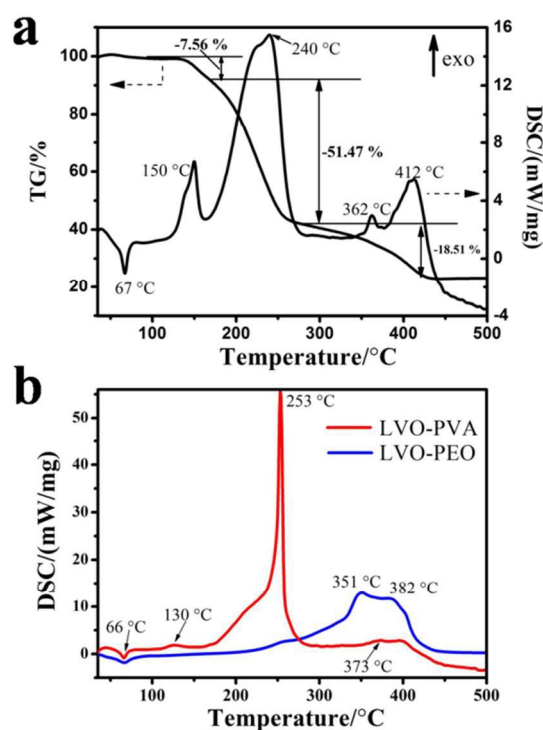
Fig. 5 (a) TG and DSC curves of the electrospun LVO-PVA/PEO composite. (b) DSC curves of the electrospun LVO-PVA and LVO-PEO composite.
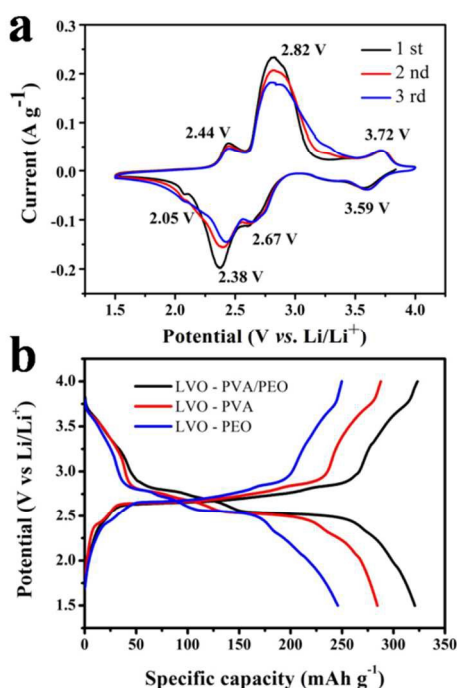
Fig. 6 (a) The CV curves of LVO-PVA/PEO at a sweep rate of 0.1 mV s^{-1} in the potential range from 1.5 to 4.0 V *vs.* Li/Li$^+$. (b) Charge–discharge curves of LVO-PVA/PEO, LVO-PVA and LVO-PEO at 100 mA g^{-1}.

Detailed electrochemical measurements were conducted to investigate the lithium storage performance. Fig. 6a shows cyclic voltammetry curve of the LVO-PVA/PEO calcined at 400 °C. The voltammograms were measured at a sweep rate of 0.1 mV s^{-1} in the potential window of 1.5 to 4.0 V at room temperature. All of these peaks originate from the phase transitions between Li$_{1+x}$V$_3$O$_8$ components with different x values (0<x<3). The cathodic peak at 3.59 V corresponds to the initial Li ion insertion into the octahedral site of the LiV$_3$O$_8$ host structure. The small peak at 2.67 V corresponds to Li ion insertion into the empty tetrahedral site through a single-phase reaction. Pan *et al.*[11] reported a similar phenomenon that the rod-shape LiV$_3$O$_8$ has relative low peak intensity at this potential. The peak at 2.38 V is related to the filling of octahedral sites formed upon intercalation during which a two-phase transition from Li$_3$V$_3$O$_8$ to Li$_4$V$_3$O$_8$ occurs. The last step at 2.05 V is attributed to the slower kinetic insertion process where the single-phase transition corresponding to the Li$_4$V$_3$O$_8$ phase takes place and all of the lithium ions are octahedrally coordinated.[30, 40] When comparing the initial three cycles of the CV curves, the partially irreversibility of phase transformation between the Li$_4$V$_3$O$_8$ and the Li$_3$V$_3$O$_8$ phases at 2.38 V caused a decrease in the discharge capacity, leading to capacity decay during cycling. Lithium insertion kinetics of Li$_{1+x}$V$_3$O$_8$ is affected largely by the small diffusivity of Li ions in Li$_4$V$_3$O$_8$ phase formed for x>1.5 upon lithiation.[41]

Fig. 6b displays the initial charge–discharge curves of LVO-PVA/PEO, LVO-PVA, and LVO-PEO cathodes measured at 100 mA g^{-1} in the range of 1.5-4.0 V. Sample LVO-PVA/PEO shows the highest discharge capacity (320 mA h g^{-1}) which is benefited from the hierarchical structure. Several plateaus are

found because of diverse phase transformations within the electrode materials during Li ion insertion/extraction. Three discharge plateaus located around 2.80, 2.65 and 2.20V can be identified as insertion of the Li ions, which result from the single-phase insertion process, the two-phase transformation from Li$_3$V$_3$O$_8$ to Li$_4$V$_3$O$_8$ and the slower kinetic insertion process, respectively. Essential information on the anodic/cathodic processes in the LiV$_3$O$_8$ electrodes can be extracted from the charge/discharge curves by translation into differential capacity curves (Fig. S8†). The anodic and cathodic peak intensities remain relative stable after cycling. The major capacity decay is due to the partially irreversibility of phase transformation between the Li$_4$V$_3$O$_8$ and the Li$_3$V$_3$O$_8$ phases which is consistent with the CV results.

Fig. 7 shows the cycling performances of three samples measured at various current densities (100, 1000, and 2000 mA g^{-1}). At the current density of 100 mA g^{-1}, the initial discharge capacity of sample LVO-PVA/PEO is up to 320.6 mA h g^{-1}, higher than those of LVO-PVA (284.3 mA h g^{-1}) and LVO-PEO (246.8 mA h g^{-1}). This is attributed to the large effective contact area supplied by the hierarchical structure. After 100 cycles, the discharge capacities decreased to 271.7, 231.3 and 157.1 mA h g^{-1}, corresponding to the capacity retention of 84.7%, 81.3% and 63.6%, respectively. The cycling performance of these three samples under high current density is further investigated. When cycled at 1000 mA g^{-1}, compared with LVO-PVA (207.2 mA h g^{-1}) and LVO-PEO (179.2 mA h g^{-1}), the LVO-PVA/PEO cathode exhibits the remarkable initial capacity of 254.0 mA h g^{-1}. After 500 cycles, the LVO-PVA/PEO cathode still delivers a discharge capacity of 129.1 mA h g^{-1}, almost two times to that of the LVO-PEO cathode (64.8 mA h g^{-1}). When current density rises to 2000 mA g^{-1}, the initial discharge capacity of LVO-PVA/PEO, LVO-PVA and LVO-PEO are 202.8, 154.5, 159.4 mA h g^{-1}, respectively. It is worth noting that the LVO-PVA/PEO cathode exhibits a remarkable capacity of 102.7 mA h g^{-1} after 500 cycles, much higher than that of LVO-PVA (69.5 mA h g^{-1}) and LVO-PEO (57.2 mA h g^{-1}) cathodes, indicating the excellent high-rate capability. Obviously, LVO-PVA/PEO electrode exhibits the highest capacity and best cycling performance under both low and high current density. Fig. 7d shows the rate performance of LVO-PVA/PEO from 100 to 2000 mA g^{-1}. Notably, the electrode shows stable capacities at each state and still provides a specific discharge capacity of 110 mA h g^{-1} even at 2000 mA g^{-1}. When rate is turned back to 100 mA g^{-1}, a specific discharge capacity of 274.8 mA h g^{-1} still can be obtained, indicating the robust structure stability. The lithium storage performance of recently published LiV$_3$O$_8$ based cathode materials are summarized in Table S1.

The advantage of hierarchical nanowire-in-network structure is further verified by the comparison of the EIS results of LVO-PVA/PEO, LVO-PVA, and LVO-PEO electrodes. Before the EIS test, the cells were charged to 3.0 V and then kept at that voltage for a period of time to reach a stable state. The Nyquist plots (Fig. 8a) exhibit two semicircles in the high frequency and medium frequency region. The high frequency semicircle is related to the interface parameters such as surface film contribution and solid-electrolyte inter-phase resistance. The mediate semicircle is attributed to the charge-transfer resistance (R_{ct}), and the slope line represents the Warburg impedance (Z_w) at low frequency, which indicates the lithium-diffusion process within the electrodes.[42, 43] Obviously, the R_{ct} of LVO-PVA/PEO (32 Ω) is much smaller than that of LVO-PVA (372 Ω) and LVO-PEO (429 Ω). The suppression of R_{ct} further confirms
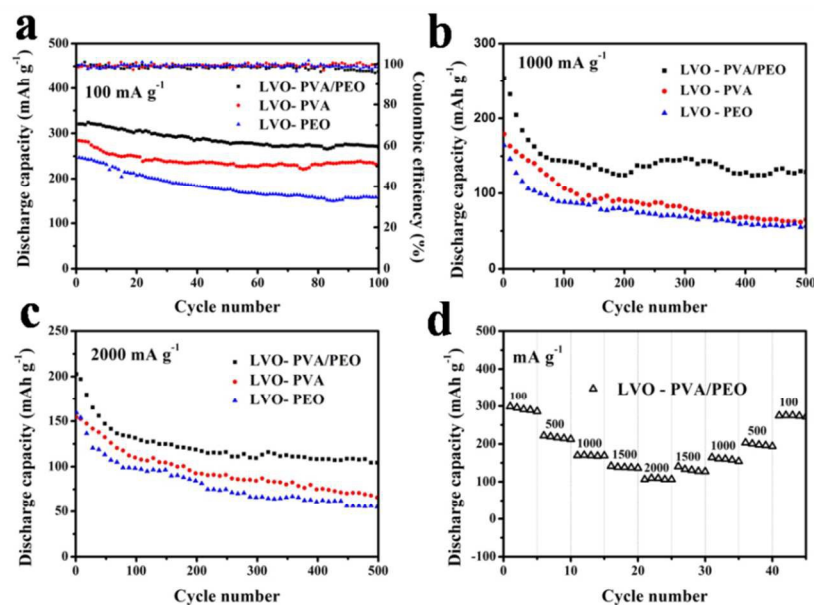
Fig. 7 Electrochemical properties of LVO-PVA/PEO, LVO-PVA and LVO-PEO. The cycling performance at the current densities of 100 (a), 1000 (b) and 2000 mA g^{-1} (c), respectively. (d) Rate performance of LVO-PVA/PEO.

that network structure indeed provides higher efficient electron/ion transport and improves the charge transfer kinetics. The slanted line is attributed to the diffusion of Li ions in the bulk of the electrode material, and the diffusion coefficient value (D) can be calculated from Equation (1) and (2).[44]

$$Z' = R_e + R_{ct} + \sigma_w \omega^{-1/2} \tag{1}$$

$$D = 0.5(RT/An^2F^2\sigma_w C)^2 \tag{2}$$
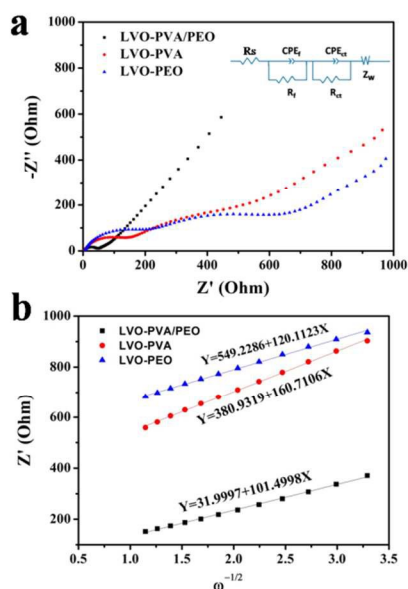
Fig. 8 (a) Nyquist plots of LVO-PVA/PEO, LVO-PVA, and LVO-PEO at 3 V and (b) the relationship curves between Z' and $\omega^{-1/2}$ in the low frequency range.

In Equation (1), $\omega(2\pi f)$ is the angular frequency in the low frequency region, and both R_e and R_{ct} are kinetics parameters independent of frequency. Then, the Warburg coefficient (σ_w) can be obtained from the slope of the fitting line (Fig. 8b). In Equation (2), R is the gas constant, T is the temperature, A is the area of the electrode, n is the number of electrons transfer per mole of the active material involved in the electrode reaction, F is Faraday's constant and C is the molar concentration of Li ions. The apparent Li ion diffusion coefficients for LVO-PVA/PEO, LVO-PVA and LVO-PEO based electrodes are calculated to be 2.30×10^{-12}, 1.64×10^{-12} and 0.91×10^{-12} cm^2 s^{-1}, respectively, indicating the faster Li ion diffusion ability of LVO-PVA/PEO.

On the basis of the above results, the hierarchical LiV$_3$O$_8$ nanowire-in-network exhibits enhanced electrochemical performance. The reasonable explanation is discussed as follows. First, the self-aggregation of small nanorods can be effectively prevented through constructing hierarchical nanowire-in-network structure, and the well-connected nanowires keep the structure more stable. Second, the width and length of each attached nanorod are around 50 nm and 150 nm, respectively. The small size of the building bloacks further realizes the advantages of nanostructured materials and improves the electrochemical performance of LiV$_3$O$_8$ electrode. Finally, the unique structure can provide continuous electron/ion conduction and extra tunnels for efficient contact between LiV$_3$O$_8$ and electrolyte compared to simple nanowire structure. Therefore, the charge transfer kinetics and cycling stability of LiV$_3$O$_8$ are promoted.

Conclusions

In summary, we have developed a facile electrospinning method to synthesize hierarchical LiV$_3$O$_8$ nanowire-in-network material. The use of polymer blends (PVA and PEO) is crucial for the formation of the structure. The LVO-PVA/PEO cathode

shows excellent electrochemical performance. When cycled at the current density of 100 mA g^{-1}, the initial discharge capacity of LVO-PVA/PEO can reach 320.6 mA h g^{-1} and still delivers a capacity of 271.7 mA h g^{-1} after 100 cycles. More importantly, the LVO-PVA/PEO exhibits outstanding rate performance (254.0 mA h g^{-1} at 1000 mA g^{-1}, 202.8 mA h g^{-1} at 2000 mA g^{-1}). This remarkable performance is attributed to the hierarchical nanowire-in-network structure, which provides large effective contact area, low charge transfer resistance and improved structure stability. Our work indicates that the crosslinking strategy in electrospinning method may be an effective way to construct unique architecture for high-performance lithium battery application.

Acknowledgements

References

1. Y. Gogotsi and P. Simon, *Science*, 2011, **334**, 917-918.
2. M. Armand and J. M. Tarascon, *Nature*, 2008, **451**, 652-657.
3. S. Chu and A. Majumdar, *Nature*, 2012, **488**, 294-303.
4. B. Kang and G. Ceder, *Nature*, 2009, **458**, 190-193.
5. J. B. Goodenough and Y. Kim, *Chem. Mater.*, 2010, **22**, 587-603.
6. A. S. Arico, P. Bruce, B. Scrosati, J. M. Tarascon and W. van Schalkwijk, *Nature Mater.*, 2005, **4**, 366-377.
7. N. A. Chernova, M. Roppolo, A. C. Dillon and M. S. Whittingham, *J. Mater. Chem.*, 2009, **19**, 2526-2552.
8. M. S. Whittingham, *Chem. Rev.*, 2004, **104**, 4271-4301.
9. C. K. Chan, H. Peng, G. Liu, K. McIlwrath, X. F. Zhang, R. A. Huggins and Y. Cui, *Nature Nanotech.*, 2008, **3**, 31-35.
10. B. Scrosati, J. Hassoun and Y. K. Sun, *Energy Environ. Sci.*, 2011, **4**, 3287-3295.
11. A. Pan, J. Liu, J. G. Zhang, G. Cao, W. Xu, Z. Nie, X. Jie, D. Choi, B. W. Arey, C. Wang and S. Liang, *J. Mater. Chem.*, 2011, **21**, 1153-1161.
12. A. Pan, J. G. Zhang, G. Cao, S. Liang, C. Wang, Z. Nie, B. W. Arey, W. Xu, D. Liu, J. Xiao, G. Li and J. Liu, *J. Mater. Chem.*, 2011, **21**, 10077-10084.
13. D. Sun, G. Jin, H. Wang, X. Huang, Y. Ren, J. Jiang, H. He and Y. Tang, *J. Mater. Chem. A*, 2014, **2**, 8009-8016.
14. L. Mai, L. Xu, C. Han, X. Xu, Y. Luo, S. Zhao and Y. Zhao, *Nano Lett.*, 2010, **10**, 4750-4755.
15. M. Zhao, B. Zhang, G. Huang, H. Zhang and X. Song, *J. Power Sources*, 2013, **232**, 181-186.
16. K. Kim, S. H. Park, T. H. Kwon, J. E. Park, H. Ahn and M. J. Lee, *Electrochim. Acta*, 2013, **89**, 708-716.
17. Y. Dong, S. Li, K. Zhao, C. Han, W. Chen, B. Wang, L. Wang, B. Xu, Q. Wei, L. Zhang, X. Xu and L. Mai, *Energy & Environmental Science*, 2015, **8**, 1267-1275.
18. L. L. Liu, X. J. Wang, Y. S. Zhu, C. L. Hu, Y. P. Wu and R. Holze, *J. Power Sources*, 2013, **224**, 290-294.
19. R. Mo, Y. Du, N. Zhang, D. Rooney and K. Sun, *J. Power Sources*, 2014, **257**, 319-324.
20. S. H. Choi and Y. C. Kang, *Chem. Eur. J.*, 2013, **19**, 17305-17309.
21. R. Mo, Y. Du, N. Zhang, D. Rooney and K. Sun, *Chem. Commun.*, 2013, **49**, 9143-9145.
22. H. Wang, Y. Ren, Y. Wang, W. Wang and S. Liu, *CrystEngComm*, 2012, **14**, 2831-2836.
23. J. Liu, K. Tang, K. Song, P. A. van Aken, Y. Yu and J. Maier, *Nanoscale*, 2014, **6**, 5081-5086.
24. L. Liang, M. Zhou and Y. Xie, *Chem, Asian j.*, 2012, **7**, 565-571.
25. Q. An, Q. Wei, P. Zhang, J. Sheng, K. M. Hercule, F. Lv, Q. Wang, X. Wei and L. Mai, Small, 2015, DOI: 10.1002/smll.201403358.
26. A. Greiner and J. H. Wendorff, *Angew. Chem. Int. Ed.*, 2007, **46**, 5670-5703.
27. C. L. Zhang and S. H. Yu, *Chem. Soc. Rev.*, 2014, **43**, 4423-4448.
28. B. Sun, Y. Z. Long, H. D. Zhang, M. M. Li, J. L. Duvail, X. Y. Jiang and H. L. Yin, *Prog. Polym. Sci.*, 2014, **39**, 862-890.
29. T. H. Hwang, Y. M. Lee, B. S. Kong, J. S. Seo and J. W. Choi, *Nano Lett.*, 2012, **12**, 802-807.
30. X. Xu, Y. Z. Luo, L. Q. Mai, Y. L. Zhao, Q. Y. An, L. Xu, F. Hu, L. Zhang and Q. J. Zhang, *NPG Asia Mater.*, 2012, **4**, e20.
31. L. Li, N. Chen, Q. Wang, *J. Polym. Sci., Part B: Polym. Phys.*, 2010, **48**, 1946-1954.
32. R. Tossici, R. Marassi, M. Berrettoni, S. Stizza and G. Pistoia, *Solid State Ionics*, 1992, **57**, 227-234.
33. L. De Picciotto, K. Adendorff, D. Liles and M. Thackeray, *Solid State Ionics*, 1993, **62**, 297-307.
34. K. P. Lee, K. M. Manesh, K. S. Kim and A. I. Gopalan, *J. Nanosci. Nanotechnol.*, 2009, **9**, 417-422.
35. A. Koski, K. Yim and S. Shivkumar, *Mater. Lett.*, 2004, **58**, 493-497.
36. J. S. Park, J. W. Park and E. Ruckenstein, *Polymer*, 2001, **42**, 4271-4280.
37. M. Krumova, D. Lopez, R. Benavente, C. Mijangos and J. Perena, *Polymer*, 2000, **41**, 9265-9272.
38. S. A. Theron, E. Zussman and A. L. Yarin, *Polymer*, 2004, **45**, 2017-2030.
39. H. G. Wang, D. L. Ma, Y. Huang and X. B. Zhang, *Chem. Eur. J.*, 2012, **18**, 8987-8993.
40. A. Sakunthala, M. Reddy, S. Selvasekarapandian, B. Chowdari and P. C. Selvin, *J. Phys. Chem. C*, 2010, **114**, 8099-8107.
41. J. Kawakita, T. Kato, Y. Katayama, T. Miura and T. Kishi, *J. Power Sources*, 1999, **81**, 448-453.
42. H. Song, Y. Liu, C. Zhang, C. Liu and G. Cao, *J. Mater. Chem. A*, 2015, **3**, 3547-3558.
43. H. Ma, Z. Yuan, F. Cheng, J. Liang, Z. Tao and J. Chen, *J. Alloys Compd.*, 2011, **509**, 6030-6035.
44. H. Wang, K. Huang, Y. Ren, X. Huang, S. Liu and W. Wang, *Journal of Power Sources*, 2011, **196**, 9786-9791.

Table of contents
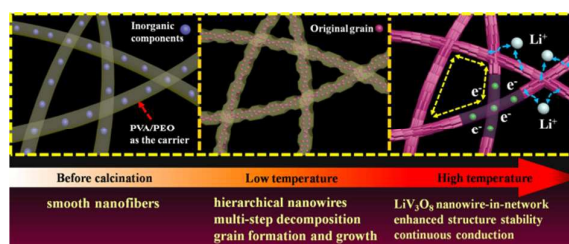
Hierarchical LiV$_3$O$_8$ naowire-in-network is synthesized via crosslinking electrospinning which provides enhanced electrochemical performance for lithium battery.